Electronic Supplementary Material (ESI) for Journal of Materials Chemistry C.

Supporting Information

A highly sensitive and flexible capacitive pressure sensor based on an ionic hydrogel dielectric layer with Lateral-bending microstructures

HaiDi Qiao[1], *Xia Liu*[1]*, *JiaYue Zhang*[2], *MingJie Yin*[2], *QingSheng Yang*[1]

1 Beijing Key Laboratory of Nonlinear Vibrations and Strength of Mechanical Structures, Beijing University of Technology, Beijing, 100124, China

2 Beijing Key Laboratory for Green Catalysis and Separation, Department of Chemical Engineering, Beijing University of Technology, Beijing, 100124, China

*Corresponding Author

Xia, Liu: liuxia@bjut.edu.cn, Fax&Tel: 0086-010-67391609

Movie S1: The movie presents the finite element simulation results of the four microstructures. To enhance the visualization of the deformation area, the microstructure depicted in the movie is scaled down to half the size of a single microstructure. The variable value, UVARM8, corresponds to a parameter defined by the UVARM subroutine in ABAQUS. In this context, the red areas indicate the deformed elements where their stress values exceed 1.1 times the target stress value. The green sections represent deformed elements with stress values ranging from 0.9 to 1.1 times the target stress value. The blue parts signify deformed elements with stress values below 0.9 times the target stress value. The target stress value is set at 0.25 MPa, and element stresses are evaluated based on the J_2 invariant.

Movie S2: The movies present various experimental setups and procedures for testing the capacitive pressure sensor. 1) Muscle motion detection: the capacitive pressure sensor, featuring the lateral-bending microstructure on its dielectric layer and equipped with copper tape electrodes, was attached to the experimenter's throat. This setup enabled the detection of muscle expansion and contraction during breathing and fist clenching activities. 2) Elbow joint flexion analysis: the sensor was secured to the elbow joint with adhesive tape. Following this, the arm was cycled through bending motions at approximately 20°, 30°, and 40° to evaluate the sensor's response to joint flexion. 3) Forearm pressure monitoring: the sensor with copper tape electrodes was attached to the forearm to monitor pressure variations due to muscle activity or external forces. 4) Finger flexion and extension test: the sensor was mounted on an index finger of a rubber glove. Connected to an impedance analyzer via a copper wire, the finger was repeatedly bent at 20°, 30°, and 40° to assess the sensor's sensitivity to finger movements. 5) Light response and durability test: The sensor was stationary on a table, and birch leaves, moistened with deionized water, were used to gently scrape the sensor's surface. This test was conducted to measure the sensor's response to light touch and its durability. 6) High pressure test: the sensor was securely affixed to the wrist of an experimenter. In this scenario, a high pressure of approximately 15 kPa was applied to the sensor surface. This controlled application of pressure was maintained for a specific duration to simulate extreme conditions that the sensor might encounter in real-

world, high-pressure applications.

Movie S3: This movie demonstrates the influence of beakers and deionized water on external detection inductors. Firstly, an external detection inductor, developed in-house, is connected to the impedance analyzer and the inductance signal response of the external inductor within the frequency range is tested. The frequency range is set to 1 MHz-20 MHz, in series mode, with a voltage of 1 V. Next, a beaker, cleaned with deionized water, is placed on an external inductor. The distance between the external detection inductor and the beaker is about 5 mm, and frequency scanning of the external inductor is carried out. Finally, 150 mL of deionized water is poured directly into the beaker and a frequency sweep test is performed again.

Movie S4: The movie analyzes the impact of deionized water on the LC resonant circuit. Firstly, the beaker and LC resonant circuit are placed on the external detection inductor, about 5 mm away from the external detection inductor. To compare the results more clearly, the sweep frequency is set to 1 MHz - 6 MHz, and the rest of the settings are identical to those in Movie S3. The sweep response of the external detection inductor is measured. Subsequently, the scanning signal response of the external detection inductor is sequentially tested, when a total of 10 mL, 20 mL, 40 mL, 80 mL, and 100 mL of deionized water are added to the beaker.

Steps to ensure optimal adhesion and performance. Initially, following the fabrication of the micro-structure ionic hydrogel using a digital light processing 3D printer, we meticulously absorb any residual uncured precursor solution from the microstructure surface using paper towels. This preliminary step is crucial for removing excess material that could interfere with adhesion. Subsequently, we expose the microstructure surface to a 365-nanometer ultraviolet (UV) flashlight for an additional 5 to 10 seconds. This supplementary curing process further solidifies the microstructure surface, reducing the potential for adhesion issues between the partially uncured microstructure and the sensor's electrode plate. Finally, we apply a minimal amount of lubricating grease to the electrode plate of the sensor. This light coating serves to facilitate a consistent contact interface without compromising the sensor's performance.

Figure S1 The influence of the structural parameters on the deformation

characteristics of the Lateral-bending microstructure was analyzed. The compression loads and contact areas of the Lateral-bending microstructures, with specific structural parameters, were computed using the ABAQUS finite element simulation software (**Figure S1**). The initial tilt angle, θ_0, and the corner radius, R_0, were found to have an impact on the deformation of the Lateral-bending microstructure, which is manifested as the change in contact area under the same compression load. The relationship between the contact area and load remained constant regardless of changes in thickness, w_0, indicating that the sensitivity of the Lateral-bending microstructure is minimally affected by variations in thickness. Furthermore, the width, x_0, of the Lateral-bending microstructure significantly affects the deformation of the arms, thus effectively reducing the required load at the same contact area. Overall, the selection of structural parameters for the preparation of the Lateral-bending microstructure is based on the design principle of a larger contact area under smaller loads.

Figure S2 shows the variations in the fraction of elements within each dielectric layer that reached a critical stress level of 0.25 MPa (Counting Criteria Shown in Movie S1 Introduction, Supporting Information.). The target stress percentage refers to the ratio of the total number of Mises stress values of elements reaching the target stress during microstructure deformation to the overall number of microstructure elements. The LB-DL exhibited the lowest number of elements reaching critical stress compared to other dielectric layers. Notably, when the displacement reached 0.16 mm, there was a substantial increase in the number of elements within the cylindrical microstructured dielectric layer that reached critical stress.

Figure S3 shows precursor solutions containing different masses of calcium chloride. It is evident that when the amount of calcium chloride added is 4.375g, the precursor solution becomes turbid and reaches a solution dissolution saturation state.

Figure S4 shows the electromechanical properties of ionic hydrogels with different calcium chloride masses. As the content of calcium chloride increases, the mechanical properties decrease. Mainly due to excessive calcium chloride affecting the cross-linking of the polymer network. However, with the increase of calcium chloride content, the capacitance of the capacitor composed of ionic hydrogel gradually

increases. Considering a minor impact on mechanical performance, the final addition amount was chosen as 3.75g of calcium chloride.

Figure S5 shows the LC wireless detection circuit, which includes the LC circuit, external detection inductance, and a beaker for storing deionized water.

Figure S6 shows the frequency-dependent of the capacitive sensor.

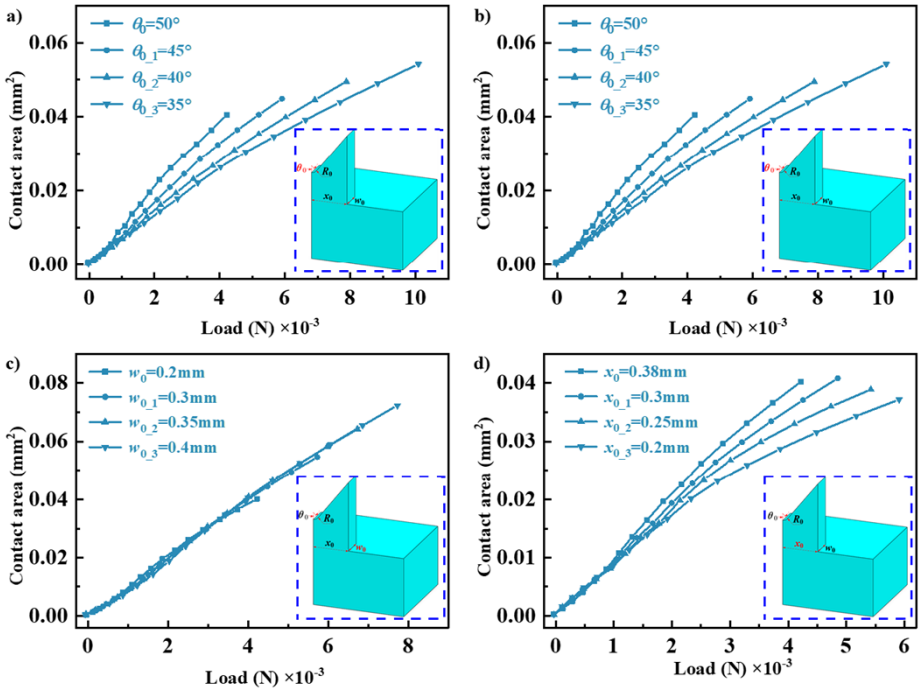

Figure S1. Influence of structural parameters on the contact area-load relationship of the lateral bending microstructure: (a) tilt angle θ_0, (b) corner radius R_0, (c) thickness w_0 and (d) width x_0.

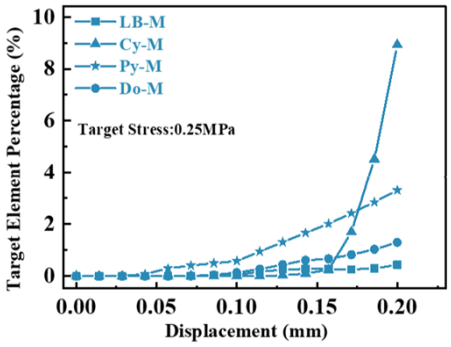

Figure S2. The changing trend of the proportion of elements in four types of microstructure finite elements.

Figure S3. Precursor solutions with different $CaCl_2$ mass configurations.

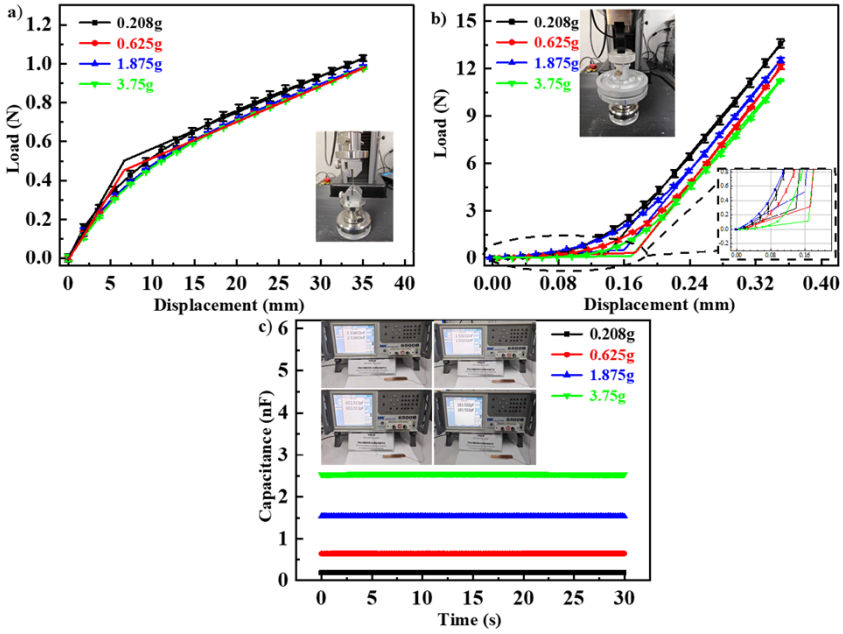

Figure S4. Effects of different amounts of added $CaCl_2$ in the precursor solution on the a) tensile and b) compressive mechanical properties, and c) electrical signals of the ionic hydrogels.

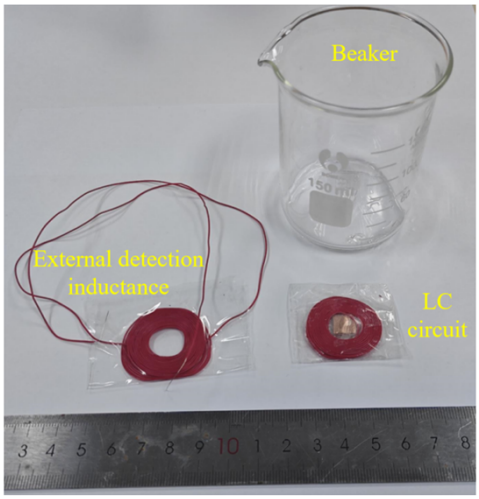

Figure S5. LC wireless detection device

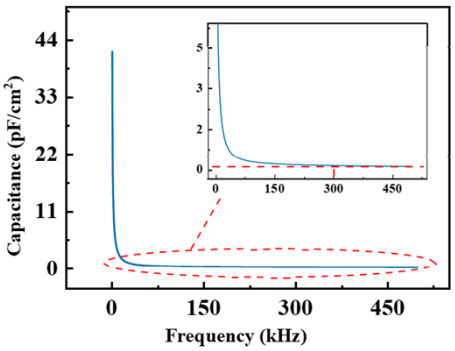

Figure S6. The trend of capacitance value per unit area within a certain frequency range.